



HHS Public Access

Author manuscript

J Colloid Interface Sci. Author manuscript; available in PMC 2019 May 15.

Published in final edited form as:

J Colloid Interface Sci. 2018 May 15; 518: 174–183. doi:10.1016/j.jcis.2018.02.030.

Modified two-step emulsion solvent evaporation technique for fabricating biodegradable rod-shaped particles in the submicron size range

Hanieh Safari^a, Reheman Adili^d, Michael Holinstat^{d,e}, and Omolola Eniola-Adefeso^{a,b,c,*}

^aDepartment of Chemical Engineering, University of Michigan, Ann Arbor, MI 48109, United States

^bDepartment of Biomedical Engineering, University of Michigan, Ann Arbor, MI 48109, United States

^cMacromolecular Science and Engineering Program, University of Michigan, Ann Arbor, MI 48109, United States

^dDepartment of pharmacology, University of Michigan, Ann Arbor, MI 48019, United States

^eDepartment of Cardiovascular Medicine, Samuel and Jean Frankel Cardiovascular Center, University of Michigan, Ann Arbor, MI 48109, United States

Abstract

Hypothesis—Though the emulsion solvent evaporation (ESE) technique has been previously modified to produce rod-shaped particles, it cannot generate small-sized rods for drug delivery applications due to the inherent coupling and contradicting requirements for the formation versus stretching of droplets. The separation of the droplet formation from the stretching step should enable the creation of submicron droplets that are then stretched in the second stage by manipulation of the system viscosity along with the surface-active molecule and oil-phase solvent.

Experiments—A two-step ESE protocol is evaluated where oil droplets are formed at low viscosity followed by a step increase in the aqueous phase viscosity to stretch droplets. Different surface-active molecules and oil phase solvents were evaluated to optimize the yield of biodegradable PLGA rods. Rods were assessed for drug loading via an imaging agent and vascular-targeted delivery application via blood flow adhesion assays.

*Corresponding Author: Department of Chemical Engineering, University of Michigan, North Campus Research Complex B028/Rm. G046W, 2800 Plymouth Road Ann Arbor, MI 48109, lolaa@umich.edu, phone: +1-734-936-0856, fax: +1-734-764-7453.

Publisher's Disclaimer: This is a PDF file of an unedited manuscript that has been accepted for publication. As a service to our customers we are providing this early version of the manuscript. The manuscript will undergo copyediting, typesetting, and review of the resulting proof before it is published in its final citable form. Please note that during the production process errors may be discovered which could affect the content, and all legal disclaimers that apply to the journal pertain.

Author Contributions

The manuscript was written through contributions of all authors. All authors have given approval to the final version of the manuscript.

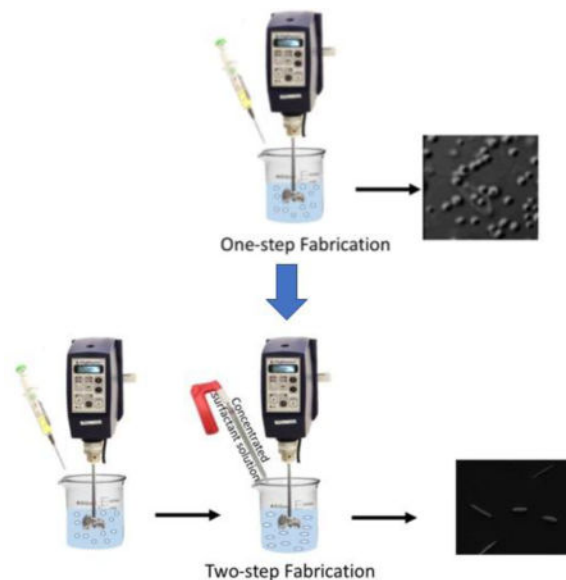
‡

Declaration of interest

Conflicts of interest: none

Findings—The two-step ESE method generated PLGA rods with major and minor axis down to 3.2 μm and 700 nm, respectively. Chloroform and sodium metaphosphate was the optimal solvent and surface-active molecule, respectively, for submicron rod fabrication. Rods demonstrated faster release of Nile Red compared to spheres and successfully targeted an inflamed endothelium under shear flow *in vitro* and *in vivo*.

Graphical abstract



Keywords

Rods; biodegradable; emulsion solvent evaporation; PLGA

1. Introduction

Biodegradable polymeric particles are widely proposed for encapsulation of therapeutics, including drugs and genes, and imaging agents in disease treatment [1]. Ideally, these particles can target and deliver the drug/imaging cargo with higher specificity to a diseased site while simultaneously providing lower systemic toxicity and improved bioavailability (circulation) compared to free drugs [1]. To date, most studies have used spherical particles for drug delivery applications for their ease of fabrication and well-studied behavior. However, there are demonstrated benefits to utilizing non-spherical shapes for targeted drug delivery applications [2]. For example, rod-shaped particles have been shown to have increased circulation time [3], slower phagocytic uptake, and lower immune clearance rate as compared to spheres [4]. Furthermore, *in vitro* and *in vivo* studies have shown that increasing the aspect ratio of microparticles enhances their vascular adhesion to endothelial cells from human blood flow, due to their larger surface area to volume ratio, which allows a larger contact area, and hence more surface-bound targeting ligands, with their target cell [5–7]. Similarly, theoretical and experimental studies show rods have improved drift towards the vessel wall and increased margination in shear flow, which increases their adhesion probability to endothelium enhancing their performance relative to spheres [8–11]. Also,

rods are shown to experience lower shear removal forces when attached to the vascular wall due to smaller drag forces [9,12]. These studies demonstrate the benefit of utilizing rod-shaped polymeric particles to increase their targeting efficiency, yet there remain challenges to developing a high throughput method to fabricate rods on the scale possible with spheres.

The current methods for the fabrication of non-spherical drug carriers include heat-stretching of spheres, template-based molding, and microfluidic techniques [13–19]. However, non-spherical particles formed via the heat-stretching of drug-loaded spherical particles [13] would likely suffer from drug degradation and leaching [14]. Similarly, template-based methods that give an accurate control over particle geometry [15,16] often require expensive and complicated setup, leading to scale up issues. Microfluidic techniques that precisely shape liquid droplets to make particles of different geometries with high control over particle size [17,18] also need complicated setups that cannot easily convert to large-scale production. An electrohydrodynamic jetting method has also been described where polymeric rods are achieved via co-spinning liquid jets into bundles followed by the cutting of the microfiber bundles into the desired size [19]. Despite having the capability of making multicompartamental particles, this approach requires complex, and specialized instrumentation and the extensive sonication used in washing steps can leach out the therapeutic loading. Thus, a need remains for a simple, inexpensive, and highly scalable technique for fabricating rod-shaped biodegradable particles.

The emulsion solvent evaporation (ESE) technique is a simple and scalable technique widely used for fabrication of spherical drug carriers [20]. We previously demonstrated that this method could be modified to fabricate rod-shaped particles with high throughput, where rods are achieved by stretching the emulsion droplets through the application of shear stress in a system with low interfacial tension [21]. However, previous studies with the ESE method have been limited to rods with major axes above 10 μm or minor axes in the micrometer range [21–24]. A long major axis for rods may impose the risk of embolism in small human capillaries when used in clinical application. Thus, there remains an interest in the development of methods that can produce smaller, biodegradable rods in a high-throughput manner for use in clinical drug delivery applications. Previous attempts to obtain smaller rod sizes with the standard ESE method have not been successful; the droplets are either not capable of being stretched or have resulted in other shapes, e.g. rhombus shape with unsmooth surface morphologies [21,22]. This limitation to produce smaller rods result from the stretching of oil droplets being a product of the competition between the shear forces and the capillary forces in ESE method as defined by droplet dynamics [25]. Two dimensionless numbers control droplet deformation during the oil-water emulsification in the ESE. First, the capillary number described in Equation 1, where γ is the shear rate, η_s is the water phase viscosity, a is the droplet radius, and Γ is the interfacial tension between the oil phase and the water phase [26], and second, the viscosity ratio of the water phase to oil phase [21].

$$\text{Ca} = \frac{\gamma \eta_s a}{\Gamma} \quad (1)$$

Lowering viscosity ratio and increasing Ca results in better droplet deformation. Thus, the smaller droplet size needed to achieve smaller rods would decrease Ca , making droplet stretching impossible even for high viscosity values.

In this study, we developed a two-step fabrication method to reduce the size of the ellipsoidal particles fabricated by the ESE while maintaining the scalability and high yield characteristics of the technique. Small-sized droplets are formed in the first step, followed by a step change in the viscosity of the fabrication system to enable the stretching of small droplets into rod particles in the second stage. With optimization of the two-step process, we were able to fabricate biodegradable, poly(lactic-co-glycolic acid) (PLGA) rods with major and minor axes size as small as 3.2 μm and 700 nm, respectively. Furthermore, the particles were successfully loaded with Nile Red fluorescent dye, confirming the capability for loading therapeutics into the submicron rods into our two-step fabricated biodegradable particles. Importantly, this simple, bottom-up fabrication technique produces polymeric rods in size range viable for *in vivo* targeted drug delivery applications, which we demonstrated rods fitted with antibodies on their surfaces were able to bind to inflamed vascular in a microfluidic model of human blood flows and *in vivo* in mice.

2. Materials and methods

2.1. Human and Animal Study Approvals

Fresh human blood used in all *in vitro* assays was obtained via venipuncture. The blood draw protocol used was approved by the University of Michigan Internal Review Board (IRB-MED). All human subjects provided written consent before blood collection. Umbilical cords were obtained under a University of Michigan Medical School Internal Review Board (IRB-MED) approved human tissue transfer protocol, which is exempt from informed consent per federal exemption category #4 of the 45 CFR 46.101.(b).

Animal studies were conducted following the National Institutes of Health guidelines for the care and use of laboratory animals and approved by the Institutional Animal Care and Use Committee (IACUC) of the University of Michigan. C57BL/6 mice were obtained from Jackson Laboratories. All animals were maintained in pathogen-free facilities at the University of Michigan and used between three and four weeks of age.

2.2. Materials

Poly(vinyl alcohol) (PVA) (MW= 30000–70000), chloroform (anhydrous >99.0%, containing 0.5–1.0% ethanol as stabilizer), dichloromethane (DCM), Trizma base, Nile Red, Bovine Serum Albumin (BSA), N-(3-Dimethylaminopropyl)-N'-ethylcarbodiimide hydrochloride (EDAC), hydrochloric acid(36.5–38.0%, bioreagent) and sodium hydroxide were purchased from Sigma-Aldrich (St Louis, MO). Sodium tripolyphosphate was purchased from Alfa Aesar (Ward Hill, MA). Sodium metaphosphate was obtained from Fisher Chemicals (Fair Lawn, NJ). Poly (lactic-co-glycolic acid), PLGA, polymer (DLG 4.5A) was purchased from Evonik Industries (Birmingham, Al). NeutrAvidin Protein and Dulbecco's phosphate-buffered saline (DPBS) were purchased from Invitrogen (Carlsbad, CA). Dextran was purchased from Spectrum Chemical Manufacturing Corporation (New

Brunswick, NJ). Fluorescein (FITC) Goat IgG and FITC Goat Anti-Mouse IgG were purchased from Jackson ImmunoResearch (West Grove, PA). The human ICAM-1/CD54 biotinylated antibody was obtained from R&D systems (Minneapolis, MN). Biotin Rat IgG₁ λ isotype control and Biotin Rat Anti-Mouse CD62P were purchased from BD Bioscience (San Jose, CA). FITC anti-Rat IgG₁ was purchased from Novus Biologicals (Littleton, CO). Human Interleukin 1-b (IL1-b) was purchased from Fitzgerald Industries International (North Acton, MA). Recombinant Human TNF- α was purchased from BioLegend (San Diego, CA).

2.3. One-step fabrication

The one-step fabrication was completed as previously described by Heslinga et al. with minor changes [21]. Briefly, an aqueous phase was prepared by dissolving the desired concentration (1–3%) of PVA and 2.0% sodium tripolyphosphate, a surface-active molecule in deionized water; then the pH was adjusted to 8.4. The oil phase was prepared by dissolving PLGA polymer at 1.8 mg/ml concentration in 12.5 ml chloroform. The oil phase solution was then injected into 100.0 ml of the aqueous phase, which was continuously stirred at the desired speed of 2500–5500 rpm (Caframo overhead mixer, model: 6015, fitted with a 2.8 cm glass propeller; Beckman Coulter). The emulsification was continued for 2 hr to allow the stretching of the droplets and complete evaporation of the organic solvent. Spherical particles of the same size were fabricated by the same procedure except with no surface-active molecule in the aqueous phase solution. Particles were collected and washed two times by centrifugation at 3500 rpm and lyophilized. The powder was stored at –20 °C until usage.

2.4. Two-step fabrication

The first step aqueous solution was prepared by dissolving 1.0 % PVA and the surface-active molecule of choice (Trizma base, sodium tripolyphosphate or sodium metaphosphate) in DI water and adjusting the pH at 8.4. The oil phase was prepared by the same protocol as the one-step fabrication (unless otherwise specified) in 12.5 ml of chloroform or dichloromethane. The oil phase solution was injected into 50.0 ml of the aqueous phase continuously stirred (2500–5500 rpm) with the overhead mixer. The mixing was continued for 15 minutes to allow the complete formation of the emulsion droplets. The second step aqueous solution was prepared by dissolving the PVA (2.0–8.0%) and the desired surface-active molecule in DI water, setting the pH at 8.4. After 15 min of mixing, 50.0 ml of the second step solution was poured into the fabrication mixture to induce a sudden increase in the viscosity of the solution and to allow the stretching of the previously formed, spherical emulsion droplets. The emulsification was continued for 2 hr to allow the stretching of the emulsion droplets and complete evaporation of the organic solvent. The fluorescently loaded particles were fabricated in the same manner as unloaded particles except for 1.0 mg of Nile Red was dissolved along with the PLGA polymer in the oil phase. The formed particles were collected and washed by two-times centrifugation at 3500 rpm and subsequently lyophilized and stored at –20 °C until usage.

The interfacial tension between the oil phase (1.8 mg/ml PLGA in 12.5 ml Chloroform) and the water phase containing one of the different surface-active molecules at their optimum

concentration, was measured with pendant drop method using needle SNS051/026 at 21 °C by the DataPhysics company.

2.5. Particle Characterization

Brightfield and fluorescent imaging were performed with the Nikon E-800 Widefield Microscope, with 40×, 60× in DIC mode and 100× objectives. The fabrication yield and spheroid ratio were quantified by counting the number of rods and spheres in each field of view and dividing the number of rods to the total number of the particles. The reported yield is the average of 3 batches ± standard error between different batches. The particle size, reported as the average ± standard deviation, was measured with NIS-Elements (AR 4.30.01) software for at least 100 particles per batch and averaged over three batches. Statistical analysis of particle size was done via two-way ANOVA test (PRISM software). SEM micrographs were obtained with JEOL-7800FLV FE-SEM. Samples for SEM were prepared by suspending particles in DI water and allowing these to be dried on a clean glass slide. Dried particle samples were sputter coated with gold before SEM imaging. Confocal images were obtained with Olympus FV 1200 Confocal Microscope.

2.6. Particle functionalization

Particles were covalently conjugated with NeutrAvidin protein using carbodiimide (EDAC) chemistry as previously described [27] with slight modifications. Briefly, particles were incubated in 5.0 mg/ml NeutrAvidin in 50 mM MES buffer (pH=4.5) for 20 minutes. Afterwards, the same volume of 75 mg/ml EDAC in 50 mM MES buffer was added to the reaction mixture and incubated for 20 hr. The reaction was stopped with 100mM glycine. Avidin-conjugated particles were washed two times with DPBS buffer (1% BSA; pH=7.4) and stored at 4°C until use.

For antibody conjugation, avidin-coated particles were incubated in biotinylated anti-ICAM-1 or biotinylated anti-P-selectin solution in DPBS buffer for 45 minutes. Antibody-conjugated particles were then washed 2 times with DPBS and stored at 4°C until use. The antibody site density on the particles was characterized using flow cytometry with FITC-goat anti-mouse IgG and FITC-Goat IgG used for the stain and isotype control, respectively. FITC anti-Rat IgG₁ and biotin Rat IgG₁ λ isotype control were used to determine the site density of anti-P-selectin coated particles.

2.7. Quantification of therapeutic loading and encapsulation efficiency

Nile Red encapsulation efficiency was calculated by dissolving the particles in dichloromethane after fabrication. The encapsulated dye was dissolved in methanol after complete evaporation of dichloromethane and the fluorescent intensity measured with a Biotek microplate reader at an excitation and emission wavelength of 530 nm and 635 nm, respectively. The fluorescence measurements were converted to concentration using a calibration curve generated with a known concentration of the dye. Therapeutic loading is calculated by dividing the mass of the entrapped Nile Red by the mass of dry PLGA particles. Encapsulation efficiency is calculated by the ratio of the mass fraction of the dye in dried particles to the mass fraction of dye in the oil phase used for particle fabrication [21].

2.8. *In vitro* release studies

In vitro release studies of Nile-Red from the loaded particles were performed in DPBS at 37 °C. Briefly, 5×10^8 particles were suspended in 1.0 ml of DPBS and rotated on a shaker at 37 °C. At the desired time point, the particle suspension is centrifuged at 8000 rpm for 5 min and the supernatant removed to measure the amount of dye released from the particles. The fluorescence intensity of the solution is then measured and quantified as described for the quantification of therapeutic loading. The pellet was resuspended in fresh DPBS buffer and rotated for subsequent time points. The release study was performed in triplicate for each particle type.

2.9. Parallel Plate flow chamber adhesion assay

Human umbilical vein endothelial cells (HUVECs) were cultured on glass coverslips as previously described [27]. Blood from human donors was drawn with the anticoagulant acetate citrate dextrose (ACD) and stored at 37°C until use. Red Blood Cells (RBCs) were separated from collected whole blood by adding 6% dextran to the blood in an inverted syringe. RBCs were washed three times by suspending in DPBS and centrifugation at 2250 g for 20 minutes. RBC sample was then reconstituted in DPBS with 1% BSA at 40% hematocrit (% v/v). HUVECs on gelatin-coated coverslips were activated as previously described with IL-1b [27]. Targeted particles at a fixed concentration of 1×10^6 particles/mL were mixed with RBCs in buffer mixture previously prepared and then perfused through the PPFC in a laminar flow profile for 5 min. The volumetric flow rate through the channel (Q) was controlled via a syringe pump. Wall Shear Rate (WSR, γ_w) can be calculated as shown in Equation (2), where h is the channel height (0.0127 cm), w the channel width (0.25 cm), and Q the volumetric flow rate (mL/sec). Adherent particles were visually counted and normalized to the HUVEC surface area, resulting in reported #particles/mm² for all experiments. Data were averaged over ten images for each trial and repeated for three trials for each data point. Data are reported as the average \pm standard error of the mean in all figures. A two-tailed t-test on GraphPad Prism (P<0.05) was used to analyze any statistical difference between various conditions.

$$\gamma_w(S^{-1}) = \frac{6Q}{h^2W} \quad (2)$$

2.10. Intravital fluorescent microscopy

Mesentery vessels were visualized as previously described [28]. Briefly, male mice (3–4 weeks) were anesthetized. A midline incision in the abdominal cavity was made for exteriorization of the mouse intestines and the mesentery connective tissue. Mice were placed on a custom-made microscope heated stage at 37 °C, and the mesentery was positioned on a glass coverslip. A local injury was induced by topical application of TNF- α (10 μ L of 200 mg/mL in PBS). At 2 min after TNF- α activation, particles suspended in 100 μ L PBS (10^8 particles/mice) were injected using retro-orbital injection and continuously imaged for another 10 minutes via both brightfield and fluorescent microscopy. Targeted particle adhesion in mesenteric veins was visualized under a 25 \times oil objective using an inverted fluorescence microscope (Zeiss Axio Observer Z1 Marianas Microscope). Adhesion

data were determined by the number of individually bound particles for $n=3$ mice and reported as #of bound particles/mm² mice vessels.

3. Results and discussion

3.1. Effect of droplet size on the yield of ESE technique

The ESE method typically consists of the polymer of choice, PLGA, dissolved in an organic solvent, which is emulsified into an aqueous phase that consists of surfactant and, in some cases, a surface-active molecule. In this work, the baseline ESE process composed of an oil phase having 1.8 mg/mL PLGA polymer dissolved in chloroform and an aqueous phase containing PVA (1%) as the surfactant and sodium tripolyphosphate (2.0%) as the surface-active molecule. The dimension of the rods obtained from the ESE method is set by the size of the initial oil droplet formed at the start of the oil-water emulsification. As such, the desired goal of achieving smaller rod dimensions requires altering the ESE process to produce smaller sized droplets. Previous reports have shown that increasing the surfactant concentration, lowering polymer concentration in the oil phase, and increasing the shear rate/mixing speed all yield smaller droplet size in the ESE method [21]. Indeed, increasing the shear rate for the emulsion in our system from 2500 to 5500 at fixed oil and water phase conditions resulted in smaller-sized particles as shown in Figure 1a. However, as anticipated, the increase in stirring speed resulted in a decrease in the yield of rods from 66% to 8% (Figure 1b) due to smaller droplet size significantly lowering the Ca (Equation 1) to below the threshold required for droplet deformation.

Another way to boost the Ca while maintaining small droplet size is by increasing the viscosity of the system, which can be achieved by increasing the surfactant, PVA, concentration in the oil phase. Figures 1c and 1d demonstrate the size and yield of rods fabricated with increasing concentration of PVA in the water phase at a fixed stir rate of 4500 rpm. All other process conditions are as for the data presented in Figures 1a and b. As expected, an increase in the surfactant concentration from 1.0 to 3.0% decreased the major axis size from 5.5 to 4.0 μm , but the particle yield dropped from 40% to 20%. Again, the observed decrease in the yield is due to a reduction in the droplet size with the now higher water phase viscosity leading to a lower Ca . These results demonstrate the interdependency of the various parameters that contribute to droplet dynamics and that the ESE technique would need to be significantly modified to allow fabrication of rod particles in the submicron size range required for drug delivery applications.

3.2. Modified two-step solvent evaporation fabrication technique

Due to the difficulty of stretching smaller sized emulsion droplets by the simple, one-step ESE technique, we sought to modify this method to fabricate smaller-sized rods. Thus, we developed a two-step fabrication method, where the droplet formation and elongation step are temporally separated from each other. In the first step, the droplets are formed, and the size fixed with a low surfactant concentration corresponding to lower aqueous phase viscosity. Next, a solution with a higher surfactant concentration is added to the aqueous phase to create a step increase in the viscosity of the water phase. This sudden increase in viscosity translates to a rise in the system Ca and decrease in the viscosity ratio, both of

which favor droplet deformation and, hence, increases in the rod fabrication yield. Also, a higher viscosity will result in slower solvent removal rate, allowing more time for the droplets to be stretched. We compared the fabrication yield between the one- and two-step method for different concentrations of PVA (surfactant) used in the second step at a fixed stir rate of 5500 rpm and with the baseline condition used for the oil phase and surface-active molecule. Figure 2a shows the percent rod formed as the PVA concentration in the water phase of the second step is set at 2% or higher for a fixed first step PVA concentration of 1.0%. Our results demonstrated a significant increase in the rod yield for the two-step fabrication system when the PVA concentration of the second step water phase is set at 3% or higher (Figures 2a). The maximum rod yield of 55% was observed at the second-step PVA concentration of 6.0%, which represents a 5-fold increase in the yield compared to the one-step process (Figures 2a and S1). Figure 2b shows that the size and the aspect ratio of the rods produced did not change with the change in the second step PVA concentration, verifying the hypothesis that the droplet size is fixed in the first step of the two-step process. Indeed, other works have characterized droplet formation in the ESE and reported that the droplet size stabilizes after a specific time point and no further change in the size of the particles is observed with continued shear [29,30].

3.3. Effect of the Oil Phase Solvent

Next, we sort to improve the ellipsoid yield for the two-step fabrication process by optimization of the material choice and fabrication system. The oil phase evaporation rate and the ratio of the oil to water phase viscosity are two parameters that contribute to the degree of stretching possible for emulsion droplets [21]. Thus, the choice of the oil phase solvent is critical to the fabrication yield. In the results presented thus far, chloroform was the solvent of choice for the oil phase. However, Dichloromethane (DCM) is another solvent used with the ESE method in a majority of previously published studies. Thus, we explored using DCM as the oil phase solvent in our two-step method. The second step PVA concentration of 6.0% that produced the maximum rod yield with chloroform was used for this comparison (with surface active molecule= 2.0% Sodium tripolyphosphate and first step PVA concentration= 1.0%). Across all the stirring speeds explored, the use of DCM as the oil phase solvent resulted in a lower particle yield compared to the yield obtained with chloroform (Figure S2) with the difference being more significant for higher stir rates, i.e. smaller droplets. Specifically, having DCM as the oil phase solvent resulted in between 7–38% decrease in the average fabrication yield relative to chloroform. Interestingly, the size of the rods, i.e. droplet size, remained the same between DCM and chloroform for all the shear rates used (Figure S3). This result can be rationalized by the fact that chloroform has a significantly slower evaporation rate compared to DCM (the vapor pressure of chloroform and dichloromethane at 25 °C is 197 and 435 mmHg, respectively [31]) while having only 23% higher viscosity (0.437 cP for DCM [32] and 0.563 cP for chloroform [33] at 20 °C). Thus, the utilization of chloroform as the oil phase solvent produces an increase in the evaporation time, translating to an increased time available for droplet stretching before droplet solidification. The near equal performance of DCM relative to chloroform at the lower stirring speeds is likely due to the droplets at lower stir speeds being large enough, enabling them to be readily stretched even in the presence of DCM [21,25].

3.4. Effect of the Surface-Active Molecule on Rod Production

The presence of a surface-active molecule enables droplet deformation via the interaction of the hydrophilic groups between the surface-active molecule and the polymer, which will lead to lower interfacial tension and hence increase in Ca . The surface-active molecule making the strongest interaction with PLGA polymer is predicted to lead to the lowest interfacial tension and thus the highest rod fabrication yield. Trizma base and sodium tripolyphosphate have been previously used in individual studies for PLGA rod fabrication [21,24]. However, different surface-active molecules have yet to be compared head-to-head in the same system to determine the properties that make the surface-active molecule favorable for use with a specific polymer choice. Here, we compared three different surface-active molecules: Trizma base, sodium tripolyphosphate (NaTP), and sodium metaphosphate (NaMP) (Figure 3a). Sodium metaphosphate was chosen as the third molecule for its similar structure to NaTP and its higher number of negatively charged oxygens per molecule, which we hypothesize would result in a stronger interaction with PLGA. To start, we determined the optimum concentration for each surface-active molecule that results in the highest fabrication yield in the two-step ESE fabrication technique. The optimum concentrations were found to be 1.2% for Trizma base (Figure 3b), 2.0% for NaTP (Figure 3c) and 3.0% for NaMP (Figure 3d). The performance of the three surface-active molecules was then compared in the two-step fabrication at their optimum concentration. The results displayed in Figure 3e demonstrate that the spheroid yield increased with the change in the surface-active molecule from Trizma to NaTP to NaMP for most stir rates evaluated and with all other process conditions fixed at baseline. Again, the size of the particles did not significantly change with the different surface-active molecules (Figure S4). Changing from NaTP to NaMP resulted in between 10–32% increase in the fabrication yield for the different shear rates, while the use of Trizma base resulted in 5–28% decrease in the rod yield relative to NaTP. The difference in the yields across different surface-active molecules is more pronounced at the higher shear rates, which again is likely due to the smaller size of the droplets at high shear rates that make the stretching process harder for the droplets – hence a more favorable interfacial interaction is needed. At low shear rates, the droplets are large enough to be readily stretched regardless of the surface-active molecule used.

The observed trend in the fabrication yield for different surface-active molecules can be explained by the chemical structure of the three molecules used (Figure 3a). The negative charge on the oxygen molecules of the phosphate groups in NaTP and NaMP will lead to a stronger interaction with the hydrophilic groups of the PLGA polymer and lower interfacial tension, favoring droplet deformation compared to the hydroxyl groups of Trizma base [21]. The slightly increased efficiency of NaMP at yielding more rods as compared to NaTP can be attributed to its increased ratio of the oxygen molecules to the sodium ions per molecular formula leading to the increased interaction with PLGA, hence better droplet deformation.

To directly relate the observed trend in rod yield to the interfacial condition during stretching, we made measurements of the interfacial tension produced by the various surface-active molecules using a pendant drop method (needle SNS051/026 at 21°C). The values of 2.46 ± 0.014 , 2.86 ± 0.04 and 2.99 ± 0.01 mN/m were obtained for NaMP, Trizma and NaTP, respectively. As anticipated, the interfacial value obtained for NaMP was

significantly lower than the values obtained for the Trizma and NaTP, confirming that the superior performance of this surface-active molecule to achieve high rod yield is due to a more favorable interfacial condition. Somewhat surprising, only a small difference was observed in the measured values between Trizma and NaTP despite the better performance of the later. It is possible that the interfacial tension obtained from the pendant drop method, which is conducted in static, does not adequately capture the condition that exists in the high shear and complex environment of particle fabrication. Indeed, we see that the trend with the measured interfacial forces better captures the trend in the rod yield when at the lowest stir rate of 2500 rpm than the trend at the higher stir rates. To summarize, NaMP was found to be the best performing surface-active molecule among the three choices to lower the interfacial tension of the fabrication system to achieve the highest possible yield of rods.

3.5. Fabrication of ellipsoids with controlled size and high yield

After systematically optimizing the solvent and surface-active molecule for two-step fabrication, we fabricated rods of different sizes by varying the polymer concentration in the oil phase. Rods were fabricated in the presence of chloroform as the oil phase solvent and 3.0% NaMP as the surface-active molecule, at 5500 rpm and first and second step PVA concentrations of 1.0 and 6.0%, respectively. Three different PLGA concentrations of 2.4, 1.8 and 1.4 mg/ml, resulted in rods with major axes ranging from 7.0 μm to 3.2 μm and minor axes ranging from 800 to 700 nm (Figure 4). The equivalent spherical diameter (ESD) for these rods is in the range of 1.0 – 1.7 μm , which is the smallest rod size to be achieved with the ESE technique to date. The fabrication yields for different sizes and polymer concentrations are summarized in Table 1, maintaining above 70% for all conditions tested. Figure 4c to 4h show the SEM micrographs of the rods with different sizes fabricated for the different oil phase polymer concentrations. (d)

3.6. Particle loading with imaging agents

To show the capability of our fabrication method for encapsulation of therapeutics, we loaded the rods with Nile Red by adding the dye to the oil phase. Figure 5a and 5b show the fluorescent and confocal image of the loaded particles. The fabrication size and yield did not show any significant difference from the non-loaded particles fabricated in the similar conditions. The encapsulation efficiency and drug loading were measured for Nile Red loaded rods with ESD=1.5 μm and were respectively equal to $25.2 \pm 1.3\%$ and 1.07 ± 0.06 wt/wt%. The release profile of Nile Red from rods of two different sizes with major axis sizes of 5.0 and 7.0 μm (ESD=1.5 and 1.7 μm) were investigated. All particles demonstrated an initial burst release continued with a slower linear release phase which is consistent with the reported release from PLGA particles [34]. As shown in the Figure 5c, rods showed a faster release than spheres. For both sizes of rods, more than 90% of the dye content is released in three days. However, it took six days for the spheres to release 90% of their cargo. These results are consistent with existing literature [34] and can be explained by the increased surface area of the rods compared to spheres of the same volume. Smaller particles show slightly faster release which is consistent with the theories of diffusion modeling which predict that the cumulative release percentage is proportional to the radius of the particles [34].

3.7. In vitro and in vivo adhesion of targeted rods to activated HUVEC monolayer

To preliminarily test the utility of the submicron rods generated for targeted drug delivery, we conjugated the particle surface with an anti-ICAM-1 antibody (~ 25000 sites/ μm^2) and evaluated their adhesion to an activated HUVEC monolayer. A laminar flow of human RBCs reconstituted in flow buffer (DPBS with 1% BSA) at the WSR of 500 s^{-1} was employed. Two different sizes of rods were used – major axes of 3.5 and 5 μm and minor axes of 700 and 800 nm, corresponding to the aspect ratios of 5 and 6, respectively. The spheres with the equivalent spherical diameter as rods were also tested. Targeted rods were capable of binding to the inflamed endothelium with similar or better adhesion level compared to spheres of equal volume (Figure 6a and b). Specifically, we found that the flow adhesion of rods increased by 18–25% compared to spheres, which is in line with the previously reported data with polystyrene rods [5]. Also, the larger rods had higher adhesion level compared to the smaller rod, which again is consistent with the previously reported data showing particles with 2–6 μm equivalent spherical diameter have enhanced adhesion compared to the 1 μm particles for both rods and spheres [7,27]. This increase in the binding is due to the enhanced margination of rods to the cell-free layer demonstrating their increased efficiency in targeting vascular wall.

To preliminarily assess the ability of the two-step generated PLGA rods to targeted a disease vasculature in the complex in vivo environment, we conjugated particles with an anti-P-selectin antibody at ~ 100000 sites/ μm^2 and injected them into mice with inflammation in their mesentery tissue. Our intravital microscopy experiments demonstrated targeted PLGA rods can successfully bind to the wall in mesentery blood vessels in live mice with no observable adverse effect (Figure 6c), which had not been possible with the micron-sized rods previously fabricated with the ESE technique. The number of adherent particles per area of the vessel was quantified and was 1347 ± 274 particles/ mm^2 .

4. Conclusions

In this study, we used the knowledge of interface and droplet dynamics to introduce a new two-step emulsion solvent evaporation (ESE) fabrication technique for generating rod-shaped, biodegradable particles in submicron size ranges. We hypothesize that the separation of the droplet formation in the traditional ESE method from the droplet stretching should enable the creation of submicron droplets in the first step that are then stretched in the second step by manipulation of the system viscosity. With the optimized two-step process, we managed to fabricate rods in the optimal size range for vascular targeting applications, which had not been previously achievable with the traditional one-step ESE technique [21,22,24]. The choice of the oil phase solvent and the surface-active molecule is shown to be critical to the fabrication yield. Chloroform as the solvent resulted in a significantly higher yield than the conventionally used dichloromethane. Sodium metaphosphate, which is proposed to have stronger interactions with PLGA hydrophilic groups, produced the lowest interfacial tension and hence the highest fabrication yield. The ellipsoidal particles were successfully loaded with Nile Red as the imaging agent and demonstrated a similar release profile as previous reports in the literature [34]. More importantly, rods could be successfully conjugated with targeting molecules, e.g. anti-P-selectin and anti-ICAM-1. We

demonstrated that targeted rods successfully bound to inflamed endothelium under shear flow in the presence of red blood cells both *in vitro* and *in vivo*. The level of adhesion observed for PLGA rods in human red blood cell flows was similar to the values previously reported for polystyrene model particles in the same size range [5]. The rods could successfully be injected into mice without blocking its vessels and were able to bind to the vascular wall when inflamed. No adverse effect of particle injection was observed for any animal. In future works, we aim to fully evaluate the capability of fabricated rods to function as a drug carrier for the delivery of therapeutics in atherosclerosis.

Supplementary Material

Refer to Web version on PubMed Central for supplementary material.

Acknowledgments

This work was supported by National Institute of Health [grant number R01HL115138 to OE-A]. Authors would like to thank M. Fish for reading the final manuscript, R.Wang from DataPhysics for assistance in interfacial tension measurement, Dr. C. Fromen, G.Lopez-Cazeres, W.Kelley, M.Gutierrez, and A.Banka for their technical assistance useful discussions and Professor Thurber's group for their help with confocal microscopy.

Abbreviations

ACD	Anticoagulant Acetate Citrate Dextrose
BSA	Bovine Serum Albumin
DCM	Dichloromethane
DPBS	Dulbecco's phosphate-buffered saline
EDAC	N-(3 Dimethylaminopropyl)-N'-ethylcarbodiimide hydrochloride
ESE	Emulsion Solvent Evaporation
ESD	Equivalent Spherical Diameter; Fluorescein (FITC)
HUVECs	Human umbilical vein endothelial cells
NaTP	Sodium tripolyphosphate
NaMP	Sodium metaphosphate
PPFC	Parallel Plate Flow Chamber
PLGA	Poly(lactic-co-glycolic acid)
PVA	Poly(vinyl alcohol)
RBCs	Red Blood Cells
WSR	Wall Shear Rate.

References

1. Panyam J, Labhassetwar V. Biodegradable nanoparticles for drug and gene delivery to cells and tissue. 2003; 55:329–347. DOI: 10.1016/S0169-409X(02)00228-4
2. Fish MB, Thompson AJ, Fromen Ca, Eniola-Adefeso O. Emergence and Utility of Nonspherical Particles in Biomedicine. *Ind Eng Chem Res.* 2015; 54(16):4043–4059. DOI: 10.1021/ie504452j [PubMed: 27182109]
3. Geng YAN, Dalhaimer P, Cai S, et al. Shape effects of filaments versus spherical particles in flow and drug delivery. 2007:249–255. DOI: 10.1038/nnano.2007.70
4. Champion, Ja, Mitragotri, S. Role of target geometry in phagocytosis. *Proc Natl Acad Sci U S A.* 2006; 103:4930–4934. DOI: 10.1073/pnas.0600997103 [PubMed: 16549762]
5. Thompson AJ, Mastria EM, Eniola-Adefeso O. The margination propensity of ellipsoidal micro/nanoparticles to the endothelium in human blood flow. *Biomaterials.* 2013; 34(23):5863–5871. DOI: 10.1016/j.biomaterials.2013.04.011 [PubMed: 23642534]
6. Namdee K, Thompson AJ, Golinski A, Mocherla S, Bouis D, Eniola-Adefeso O. In vivo evaluation of vascular-targeted spheroidal microparticles for imaging and drug delivery application in atherosclerosis. *Atherosclerosis.* 2014; 237(1):279–286. [Accessed November 9, 2015] <http://www.sciencedirect.com/science/article/pii/S0021915014014270>. [PubMed: 25286447]
7. Doshi N, Prabhakarandian B, Rea-ramsey A, Pant K, Sundaram S, Mitragotri S. Flow and adhesion of drug carriers in blood vessels depend on their shape : A study using model synthetic microvascular networks. *J Control Release.* 2010; 146(2):196–200. DOI: 10.1016/j.jconrel.2010.04.007 [PubMed: 20385181]
8. Decuzzi P, Ferrari M. The adhesive strength of non-spherical particles mediated by specific interactions. *Biomaterials.* 2006; 27:5307–5314. DOI: 10.1016/j.biomaterials.2006.05.024 [PubMed: 16797691]
9. Kelley WJ, Safari H, Lopez-cazares G, Eniola-adeieso O. Vascular-targeted nanocarriers : design considerations and strategies for successful treatment of atherosclerosis and other vascular diseases. *Wiley Interdiscip Rev Nanomed Nanobiotechnol.* 2016 Dec.8:909–926. DOI: 10.1002/wnan.1414 [PubMed: 27194461]
10. Gavze E, Shapiro M. Motion of inertial spheroidal particles in a shear flow near a solid wall with special application to aerosol transport in microgravity. *J Fluid Mech.* 1998; 371:59–79.
11. Lee S, Ferrari M, Decuzzi P. Shaping nano- / micro-particles for enhanced vascular interaction in laminar flows. *Nanotechnology.* 2009; :20.doi: 10.1088/0957-4484/20/49/495101
12. Müller K, Fedosov Da, Gompper G. Margination of micro- and nano-particles in blood flow and its effect on drug delivery. *Sci Rep.* 2014; 4(4871)doi: 10.1038/srep04871
13. Champion JA, Katare YK, Mitragotri S. Making polymeric micro- and nanoparticles of complex shapes. *Proc Natl Acad Sci.* 2007; 104(29):11901–11904. [PubMed: 17620615]
14. Williford J, Santos L, Santos JL. Biomaterials Science Shape control in engineering of polymeric nanoparticles for therapeutic delivery. 2015; :894–907. DOI: 10.1039/c5bm00006h
15. Rolland JP, Maynor BW, Euliss LE, Exner AE, Denison GM, Desimone JM. Direct Fabrication and Harvesting of Monodisperse, Shape-specific Nanobiomaterials. *J Am Chem Soc.* 2005; 127(28):10096–10100. [PubMed: 16011375]
16. Gratton SEA, Pohlhaus PD, Lee J, Guo J, Cho MJ, Desimone JM. Nanofabricated particles for engineered drug therapies : A preliminary biodistribution study of PRINT™ nanoparticles. *J Control Release.* 2007; 121:10–18. DOI: 10.1016/j.jconrel.2007.05.027 [PubMed: 17643544]
17. Xu S, Nie Z, Seo M, et al. Generation of Monodisperse Particles by Using Microfluidics: Control over Size, Shape, and Composition. *Angew Chemie.* 2005; 117(5):734–738. DOI: 10.1002/ange.200462226
18. Dendukuri D, Tsoi K, Hatton TA, Doyle PS. Controlled Synthesis of Nonspherical Microparticles Using Microfluidics. *Langmuir.* 2005; 21(6):2113–2116. [PubMed: 15751995]
19. Bhaskar S, Hitt J, Chang S-WL, Lahann J. Multicompartmental Microcylinders. *Angew Chemie Int Ed.* 2009; 48(25):4589–4593. DOI: 10.1002/anie.200806241
20. Donnell PBO, McGinity JW. Preparation of microspheres by the solvent evaporation technique. *Adv Drug Deliv Rev.* 1997; 28:25–42. [PubMed: 10837563]

21. Heslinga MJ, Mastria EM, Eniola-Adefeso O. Fabrication of biodegradable spheroidal microparticles for drug delivery applications. *J Control Release*. 2009; 138(3):235–242. DOI: 10.1016/j.jconrel.2009.05.020 [PubMed: 19467275]
22. Fan Q, Qi F, Miao C, Yue H, Gong F, Wu J. Colloids and Surfaces A : Physicochemical and Engineering Aspects Direct and controllable preparation of uniform PLGA particles with various shapes and surface morphologies. *Colloids Surfaces A Physicochem Eng Asp*. 2016; 500:177–185. DOI: 10.1016/j.colsurfa.2016.04.028
23. Heslinga MJ, Willis GM, Sobczynski DJ, Thompson AJ, Eniola-Adefeso O. One-step fabrication of agent-loaded biodegradable microspheroids for drug delivery and imaging applications. *Colloids Surfaces B Biointerfaces*. 2014; 116:55–62. DOI: 10.1016/j.colsurfb.2013.12.054 [PubMed: 24441181]
24. Li R, Li X, Liu L, Zhou Z, Tang H. High-Yield Fabrication of PLGA Non-Spherical Microarchitectures by Emulsion-Solvent Evaporation Method a. 2010; :1981–1986. DOI: 10.1002/marc.201000332
25. Larson, RG. *The Structure and Rheology of Complex Fluids*. Oxford University Press; 1999.
26. Gupta A, Sbragaglia M. Deformation and break-up of Viscoelastic Droplets Using Lattice Boltzmann Models. *Phys Rev E*. 2014; 90(2):23305.doi: 10.1016/j.piutam.2015.04.030
27. Charoenphol P, Huang RB, Eniola-adeieso O. Biomaterials Potential role of size and hemodynamics in the efficacy of vascular-targeted spherical drug carriers. *Biomaterials*. 2010; 31(6):1392–1402. DOI: 10.1016/j.biomaterials.2009.11.007 [PubMed: 19954839]
28. Fish MB, Fromen CA, Lopez-Cazares G, et al. Exploring deformable particles in vascular-targeted drug delivery: Softer is only sometimes better. *Biomaterials*. 2017; 124:169–179. [PubMed: 28209527]
29. Desgouilles S, Vauthier C, Bazile D, et al. The Design of Nanoparticles Obtained by Solvent Evaporation: A Comprehensive Study. *Langmuir*. 2003; 19(22):9504–9510. DOI: 10.1021/la034999q
30. Staff RH, Schaeffel D, Turshatov A, et al. Particle formation in the emulsion-solvent evaporation process. *Small*. 2013; 9(20):3514–3522. DOI: 10.1002/sml.201300372 [PubMed: 23606602]
31. Boublík, T., Fried, Vojt ch, Hála, Eduard. *The Vapour Pressures of Pure Substances*. Second. Elsevier; 1984.
32. Manfred, Rossberg, Lendl, Wilhelm, Pfeleiderer, Gerhard, Tögel, Adolf, Torkelson, Theodore R., Beutel, Klaus K. Ullmann's Encyclopedia of Industrial Chemistry. John Wiley & Sons; 2011. Chloromethane.
33. Prager, JC. *Environmental Contaminant Reference Databook*. New York, NY: Van Nostrand Reinhold; 1995.
34. Fattahi P, Borhan A, Abidian MR. Microencapsulation of Chemotherapeutics into Monodisperse and Tunable Biodegradable Polymers via Electrified Liquid Jets : Control of Size, Shape, and Drug Release. *Adv Mater*. 2013; 25:4555–4560. DOI: 10.1002/adma.201301033 [PubMed: 23824544]

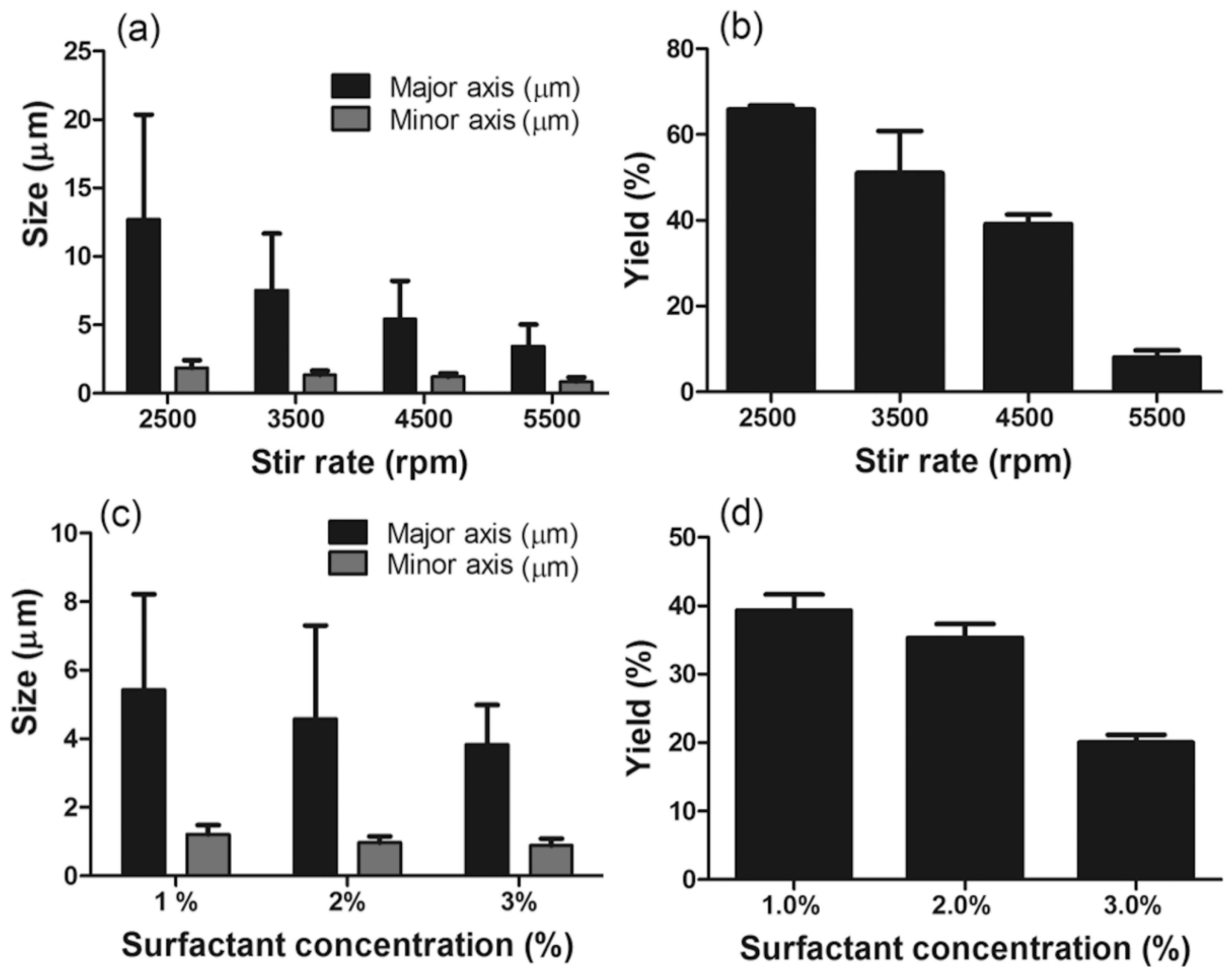


Figure 1. Rod fabrication (a) size and (b) yield as a function of stir rate in ESE technique (PVA concentration is fixed at 1.0%). Rod fabrication (c) size and (d) yield as a function of surfactant (PVA) concentration in the water phase (stir rate is fixed at 4500 rpm). For all trials, the oil phase consisted of 1.8 mg/ml of PLGA in chloroform and the water phase includes 2.0% sodium tripolyphosphate [2 column fitting image].

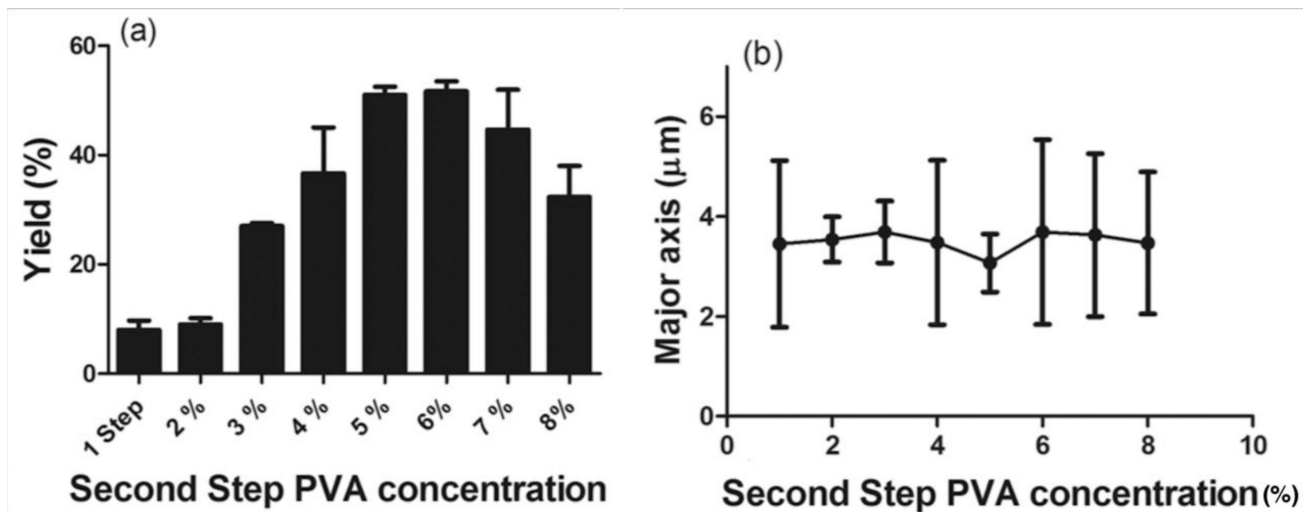


Figure 2.

Comparison of the (a) yield and (b) size for one- and two-step fabrications with different second step surfactant concentrations. The first step PVA concentration and stir rate are fixed at 1.0% and 5500 rpm. 1.8 mg/ml PLGA in chloroform and 2.0% sodium tripolyphosphate are used as the oil phase and surface-active molecule [2 column fitting image].

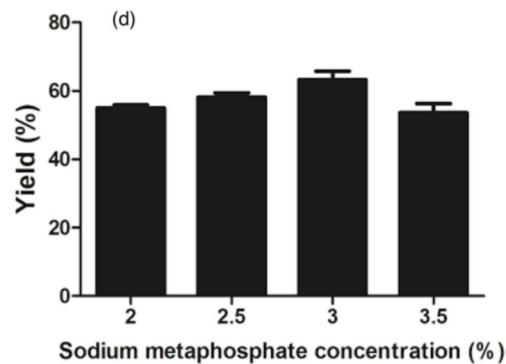
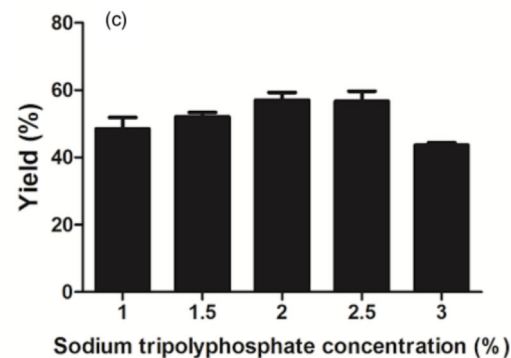
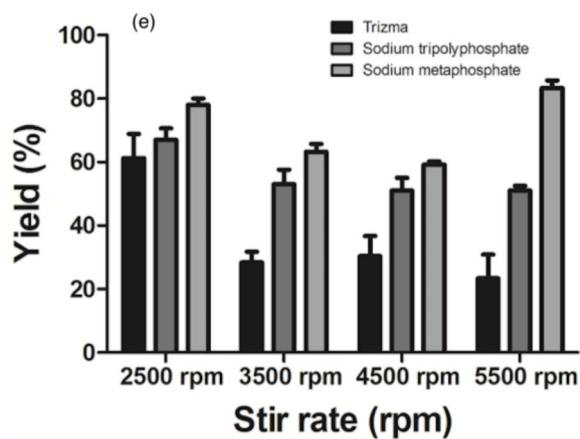
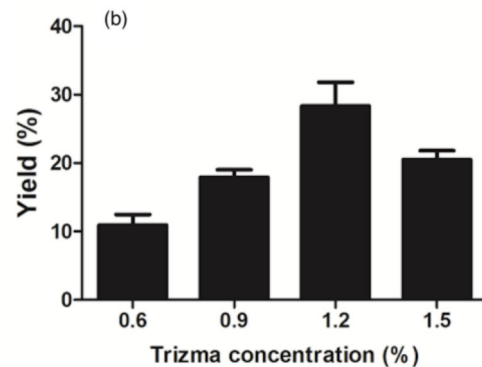
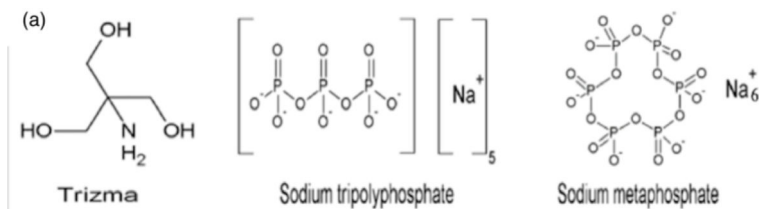


Figure 3.

Fabrication yield as a function of concentration of surface-active molecule of (a) Trizma (b) sodium tripolyphosphate and (c) sodium metaphosphate in the water phase, and (d) the choice of the surface-active molecule. (1.8 mg/ml PLGA in chloroform is used as the oil phase solvent and the first step and second step PVA concentration is fixed at 1.0% and 6.0%) (e) Chemical structure of different surface-active molecules used.

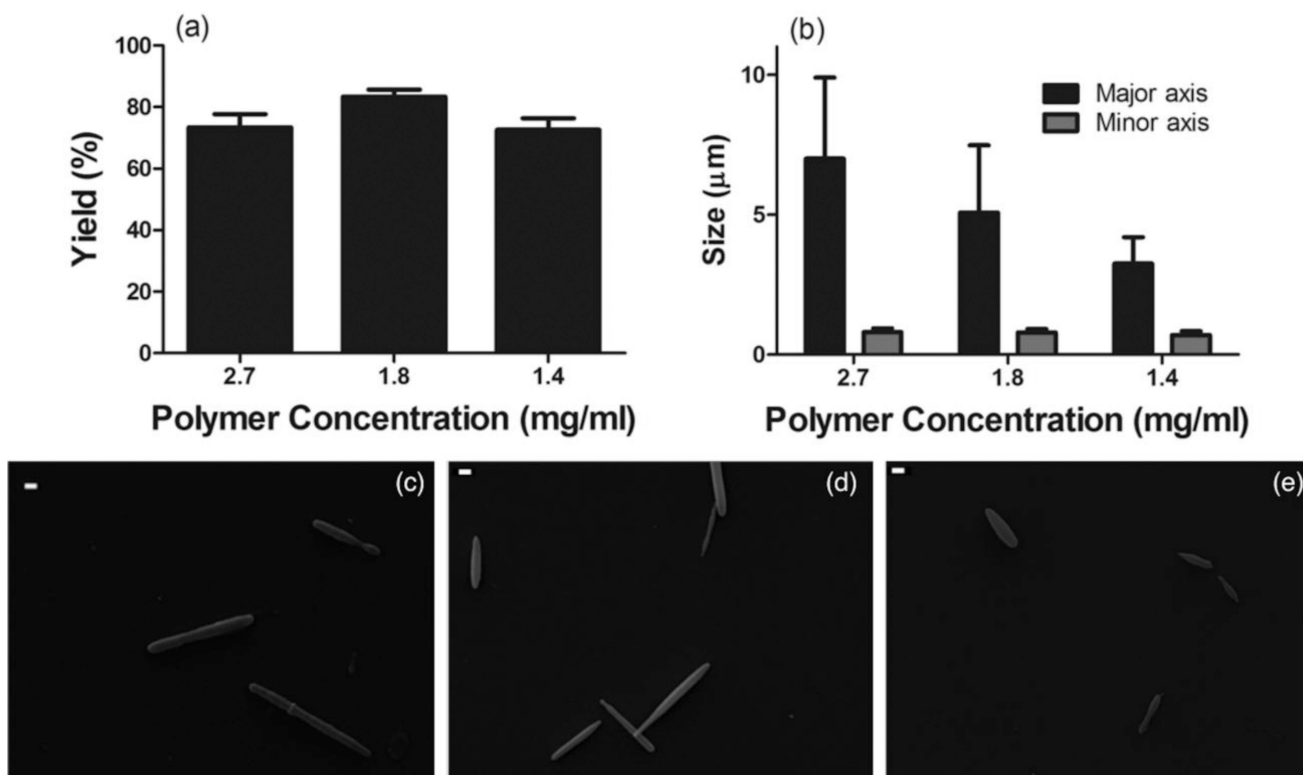


Figure 4.

(a) Yield and (b) size as a function of polymer concentration in the oil phase. Chloroform is used as the oil phase solvent and sodium metaphosphate is used as the surface-active molecule (the first and second step PVA concentration are fixed at 1.0% and 6.0%). SEM image of rods with (c) 7.0 μm, (d) 5.0 μm and (e) 3.2 μm average major axis size fabricated by two-step fabrication. Scale bars are 1.0 μm [2 column fitting image].

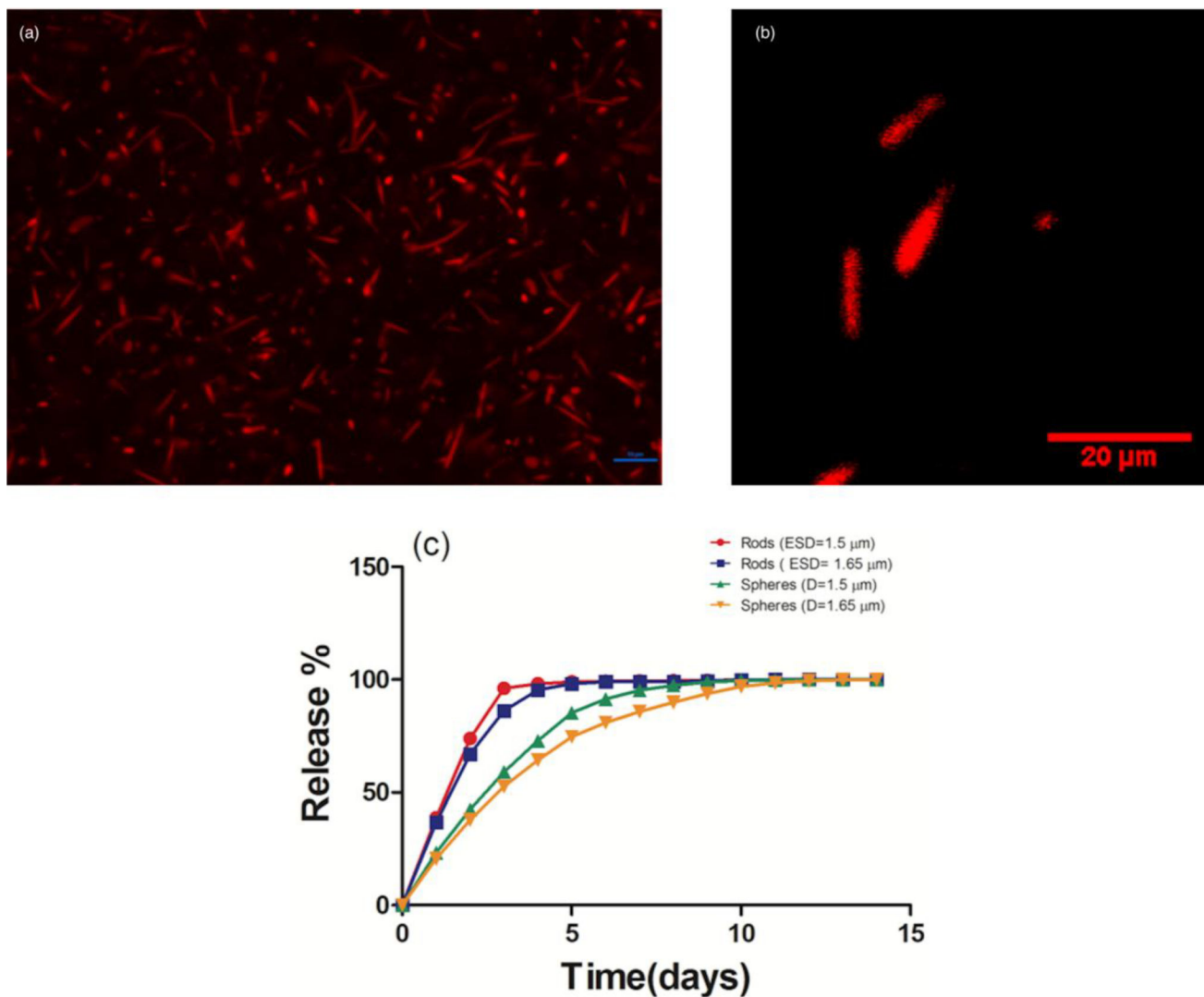


Figure 5.

(a) Fluorescent (scale bar is 10 μm) and (b) Confocal image of the rods with 5.0 μm average major axis size loaded with Nile Red. (c) The release profile of Nile Red from loaded rods and spheres of two different sizes (error bars are smaller than 1.0% for all points) [2 column fitting image, colored artwork].

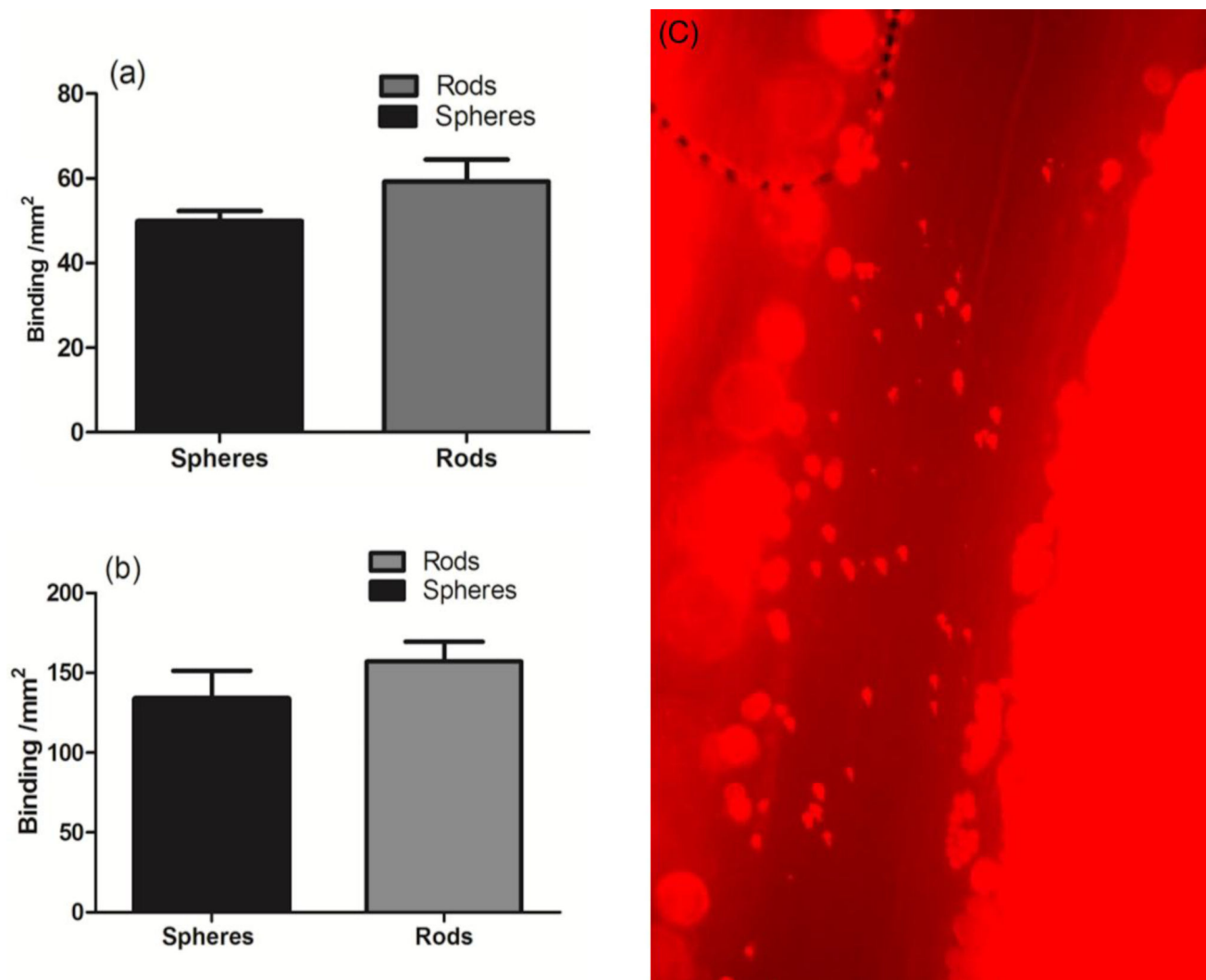


Figure 6. *In vitro* binding of (a) 1.3 μm and (b) 1.6 μm diameter spheres and rods with the equivalent volume in 40% RBCs in buffer. The experiments were performed at the 127 μm height channel and the wall shear rate (WSR) was set at 500 s^{-1} . (c) *In vivo* binding of the anti-P-selectin coated rods with major axis and minor axis size of 3.5 μm and 700 nm in mice vessels stimulated with TNF- α [2 column fitting image]

Table 1

Summary of the fabrication yield and sizes of spheroids fabricated with two-step fabrication

Polymer concentration	Average major axis size (μm)	Spheroid ratio (%)
2.4	7.0	74 ± 3.5
1.8	5.0	84 ± 2
1.4	3.2	73 ± 5

Author Manuscript

Author Manuscript

Author Manuscript

Author Manuscript